ADVANCED MATERIALS
www.advmat.de

Modulation of Metal and Insulator States in 2D Ferromagnetic VS_2 by van der Waals Interaction Engineering

Yuqiao Guo, Haitao Deng, Xu Sun, Xiuling Li, Jiyin Zhao, Junchi Wu, Wangsheng Chu, Sijia Zhang, Haibin Pan, Xusheng Zheng, Xiaojun Wu, Changqing Jin,* Changzheng Wu,* and Yi Xie*

2D transition-metal dichalcogenides (TMDCs) are currently the key to the development of nanoelectronics. However, TMDCs are predominantly nonmagnetic, greatly hindering the advancement of their spintronic applications. Here, an experimental realization of intrinsic magnetic ordering in a pristine TMDC lattice is reported, bringing a new class of ferromagnetic semiconductors among TMDCs. Through van der Waals (vdW) interaction engineering of 2D vanadium disulfide (VS_2), dual regulation of spin properties and bandgap brings about intrinsic ferromagnetism along with a small bandgap, unravelling the decisive role of vdW gaps in determining the electronic states in 2D VS_2. An overall control of the electronic states of VS_2 is also demonstrated: bond-enlarging triggering a metal-to-semiconductor electronic transition and bond-compression inducing metallization in 2D VS_2. The pristine VS_2 lattice thus provides a new platform for precise manipulation of both charge and spin degrees of freedom in 2D TMDCs availing spintronic applications.

The emergence of 2D materials, in particular the layered transition-metal dichalcogenides (TMDCs) with loose interlayer van der Waals (vdW) bonds, has fueled vigorous scientific inquiry.[1] By regulating the weak van der Waals interactions, 2D TMDC crystals and their assembled vdW heterostructures have been shown to exhibit unusual electronic properties,[1,2] which have received extensive scientific exploration especially in the field of nanoelectronics.[3] However, most of the pristine TMDCs are intrinsically nonmagnetic due to either weak magnetic coupling[4] or a lack of unpaired electrons,[5] which has limited their practice in the field of spintronics.[6] Systematic structural modulation approaches including heteroatom incorporation,[7] formation of surface dangling bonds,[8] introduction of defects,[9] and strain engineering[10] have been successfully employed to induce the signature of magnetic ordering in TMDCs. However, structural changes caused by foreign atoms or defects, inevitably give rise to complex entanglement among the lattice, orbit, charge, and spin degrees of freedom. Thus, the remaining challenge is whether intrinsic magnetic ordering can be realized in a pristine TMDC lattice framework, which is essential for not only manipulating both charge and spin degrees of freedom simultaneously, but also ensuring their stability and controllability catering for spintronic device.[11]

Among the family of 2D TMDCs, vanadium disulfide (VS_2) has attracted revived interest owing to the $3d^1$ electronic configuration of quadrivalent vanadium as well as strong electron coupling that allows collective electronic responses such as charge density wave order.[12] Theoretical investigation has

Dr. Y. Q. Guo, H. T. Deng, Dr. X. Sun, Dr. J. Y. Zhao, J. C. Wu, Prof. C. Z. Wu, Prof. Y. Xie
Hefei National Laboratory for Physical Sciences at the Microscale, and iChEM (Collaborative Innovation Centre of Chemistry for Energy Materials)
University of Science and Technology of China
Hefei, Anhui 230026, P. R. China
E-mail: czwu@ustc.edu.cn

X. L. Li, Prof. X. J. Wu
CAS Key Laboratory of Materials for Energy Conversion
School of Chemistry and Materials Sciences, and
CAS Center for Excellence in Nanoscience
University of Science and Technology of China
Hefei, Anhui 230026, China
E-mail: xjwu@ustc.edu.cn

Dr. W. S. Chu, H. B. Pan, X. S. Zheng
National Synchrotron Radiation Laboratory
University of Science and Technology of China
Hefei, Anhui 230029, P. R. China

Dr. S. J. Zhang, Prof. C. Q. Jin
Beijing National Laboratory for Condensed Matter Physics
Institute of Physics
Chinese Academy of Sciences
Collaborative Innovation Center of Quantum Matter
Beijing 100190, China
E-mail: Jin@iphy.ac.cn

DOI: 10.1002/adma.201700715

predicted the existence of intrinsic magnetic ordering in VS_2 monolayers, where the intensity of magnetic coupling can be regulated by means of strain.[12d] In this regard, 2D VS_2 provides a prospective experimental platform to realize ferromagnetic modulations in pristine TMDC lattice framework, which has been so far remained untapped. On the other hand, quantum confinement has endowed TMDCs with conceivable modulation of the bandgap.[3d] For example, enlarging the vdW spacing via exfoliation would lead to bandgap opening (widening) due to the elimination of interlayer coupling,[3a–d] while compression via external pressure would trigger metallization due to the increased overlap of chalcogen between the neighboring layers.[13] Along this line, regulation of vdW interactions grants feasible access to engineer the electronic structure of 2D ferromagnetic VS_2. Therefore, the pristine lattice of 2D VS_2 holds great promise for simultaneous manipulation of charge and spin degrees of freedom, which is central to next-generation spintronic devices based on TMDCs.

Herein, we report the experimental realization of intrinsic magnetic ordering in a pristine TMDC lattice. Through engineering the vdW interactions, few-layered VS_2 displayed intrinsic ferromagnetism along with a small bandgap opening, bringing a new class of ferromagnetic semiconductor among TMDCs. The pristine VS_2 with few-layered lattice enabled dual regulation of spin properties as well as bandgap, revealing the decisive role of vdW interactions in determining the electronic states of 2D VS_2. The new properties of few-layered VS_2 thus open a window for the burgeoning field of spintronics.

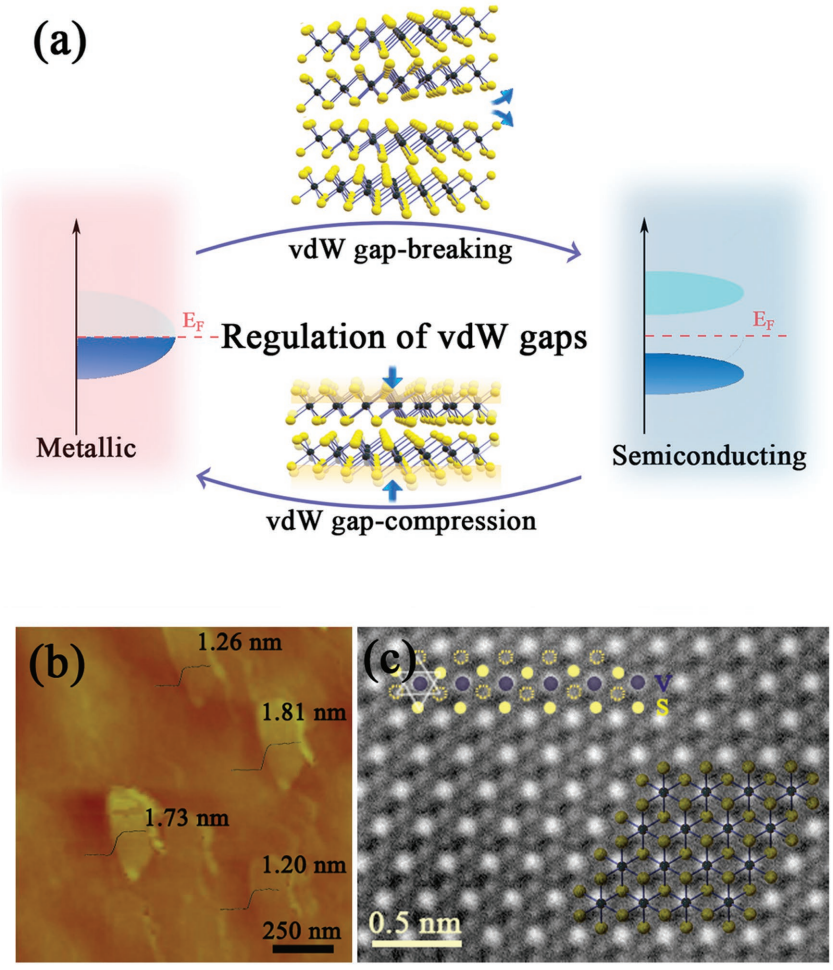

Figure 1. Overview and vdW bond-breaking by exfoliation. a) Schematic view of electronic state modulation by van der Waals interaction engineering. b,c) Atomic force microscopy (AFM) height profile and high-angle annular dark-field scanning transmission electron microscopy (HAADF-STEM) image of the exfoliated 2D VS_2 nanosheets. c) S atoms are marked in yellow (dashed and filled), while V atoms are dark violet. The inset is the top view of 1T-VS_2 crystal structure.

For tuning the spin properties and bandgap, the vdW interactions of VS_2 was engineered, as schematically illustrated in **Figure 1**a: bond-enlarging (weakening) by exfoliation triggered bandgap opening, while bond-compression (strengthening) by external-pressure-induced metallization in few-layered VS_2. Here, the exfoliation of bulk VS_2 into few-layered nanosheets and the compression (applying pressure) of few-layered nanosheets are a pair of opposite processes to regulate vdW interactions for round control of the bandgaps. The detailed methods were in the Supporting Information. Comparison of powder X-ray diffraction patterns (Figure S1, Supporting Information) indicates the successful chemical exfoliation of VS_2. All existing peaks in the diffraction patterns of the bulk sample can be indexed to 1T-VS_2 (JCPDS, No. 89-1640), ruling out the impurities, while the exfoliated nanosheets displayed a *c*-axis orientation, with only (00l) planes protruding, verifying the high quality of 2D VS_2 nanosheets. The microscopic elemental composition of the as-prepared VS_2 was further investigated via elemental mapping and energy-dispersive X-ray spectroscopy. As shown in Figure S2 (Supporting Information), the elemental composition of as-obtained products only contains V and S (Cu and C derived from Cu grid and carbon support film), and the V/S ratio is close to 1:2. The transmission electron microscopy (TEM) image (Figure S3, Supporting Information) demonstrates few-layered morphology with lateral sizes of about 400 nm. To determine the thickness of the nanosheets, the tapping mode atomic force microscopy (AFM) measurement was carried out, as presented in Figure 1b. In consideration of the lattice constant of *c* of about 0.575 nm, the VS_2 nanosheets obtained were thus mainly composed of 2–3 S-V-S trilayers. High-angle annular dark-field scanning transmission electron microscopy (HAADF-STEM) image (Figure 1c) further revealed the 1T crystal phase of VS_2, with an octahedral geometry for the metal coordination, which is well illustrated from the top view of 1T-VS_2 as an inset in Figure 1c. The above results clearly demonstrated the ultrathin character and the 1T crystal structure of the obtained 2D VS_2.

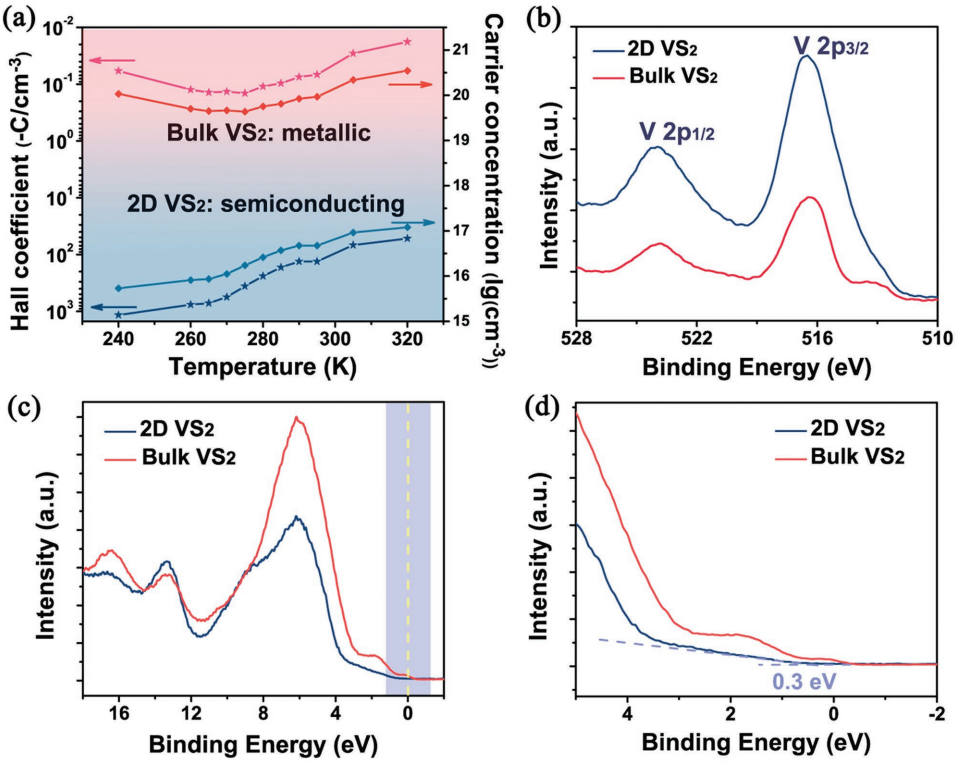

Figure 2. Bandgap opening in 2D VS_2. a) Temperature-dependent carrier concentration and Hall coefficient of VS_2. For 2D VS_2, the increase of carrier concentration with the temperature rise demonstrates semiconducting behavior. b) XPS spectra of the V 2p core level. No chemical shifts of V^{4+} were observed, ruling out the possibility of oxidation of V^{4+} or the presence of vanadium oxides. c) UPS spectra taken with synchrotron photon energy of 170 eV: full valence band, with 0 eV binding energy corresponding to the Fermi level (E_F). d) Zoomed-in view of the low-binding-energy region (c).

The electric transport properties of the 2D VS_2 were investigated by means of temperature-dependent resistivity measurements (see Methods in the Supporting information for details). Comparison of the temperature-dependent resistivity curves between 2D VS_2 and the bulk counterpart in Figure S4 (Supporting Information) indicated bandgap opening during the exfoliation process. As can be seen in **Figure 2**a, the Hall-coefficients of both bulk and 2D VS_2 are negative, indicating that the predominant carriers are electrons for both cases.[14] For bulk VS_2, the carrier concentration ($\approx 10^{20}$ cm^{-3}, typical value of a metal) derived from Hall coefficients exhibits no obvious changes with decreasing temperature, in consistence with its metallic characteristic.[15] In comparison, the steady increase in carrier concentration along with increasing temperature clearly indicates the existence of a bandgap in 2D VS_2, as more electrons were thermally activated to overcome the bandgap for electron conduction.[15b] X-ray photoemission spectra (XPS) of the V 2p core level (Figure 2b) indicate no chemical shifts of V^{4+}, excluding the oxidation process of V^{4+} or the existence of vanadium oxides. The XPS spectra of S 2p, shown in Figure S5 (Supporting information), also indicate no obvious valence state variation. To accurately investigate the band structure of VS_2, synchrotron ultraviolet photoemission spectroscopy (UPS) (the experimental setup was shown in Figure S6, Supporting Information) were carried out, from which the filled electronic states below the Fermi level or the valence band could be precisely determined. The full valence band spectrum in Figure 2c demonstrates significant changes in the low-binding-energy region, where the bulk samples have shown metallic behavior with an identifiable intensity at 0 eV (i.e., E_F). In contrast, the valence band maximum of the exfoliated 2D VS_2 occurs at 0.3 eV below E_F, as determined from zoomed-in view of the valence band spectra in Figure 2d. Hence, the 2D VS_2 nanosheets were intrinsic semiconductors, with a bandgap of 0.3 eV. The bandgap opening in 2D VS_2 could be attributed to the quantum-mechanical confinement, which eliminates the overlapping by shifting the adjacent layers in opposite directions, similar to the indirect-to-direct bandgap transition in the monolayer MoS_2.[3a,b] Consequently, engineering the vdW interactions through the elimination of vdW bonds between the neighboring layers have resulted in bandgap opening in 2D VS_2.

VS_2, due to its V^{4+} ($[Ar]3d^1$) odd electron configuration, is theoretically capable of hosting magnetic order and was thus a promising candidate for tuning the magnetic momentum in TMDC lattice.[6] We therefore performed intrinsic magnetic and magneto-transport property measurements along with the metal-to-semiconducting electronic state transition in 2D VS_2. The temperature dependence of the zero-field-cooled (ZFC) magnetization curve and the magnetic-field dependence of the magnetization (M–H curve) were measured to study the magnetic properties of few-layered VS_2 nanosheets. The ZFC curve of 2D VS_2 exhibits obvious enhancement of magnetization than that of bulk counterpart (the magnetic properties of which were

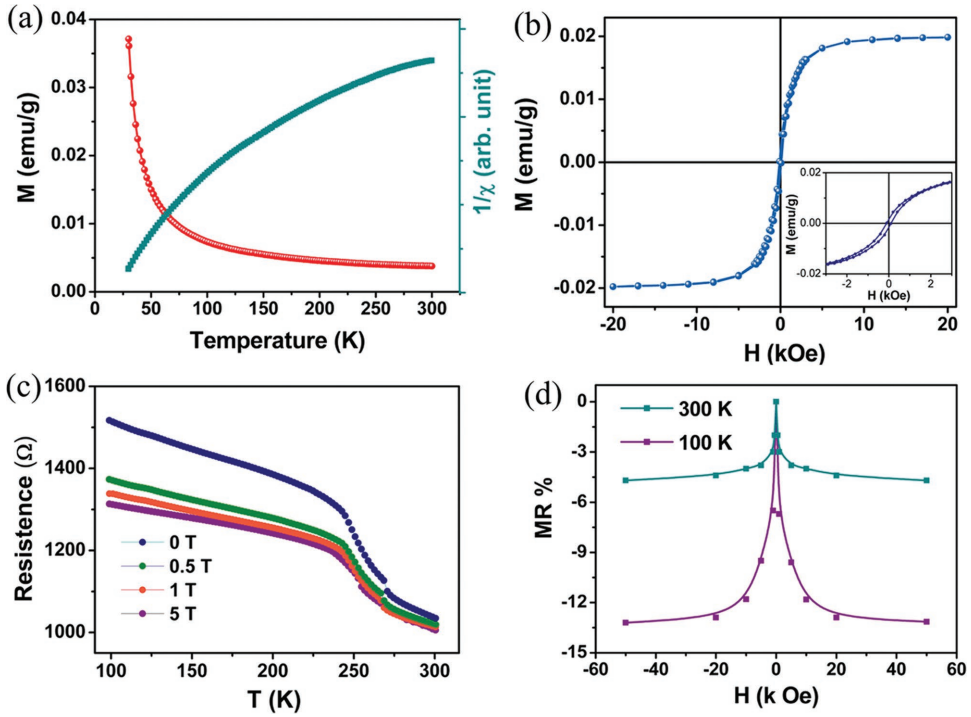

Figure 3. Intrinsic ferromagnetism and negative magnetoresistance in 2D semiconducting VS_2. a) Temperature dependence of magnetization and inverse susceptibility under zero-field cooling (ZFC) of 2D VS_2 nanosheets. b) Magnetic-field dependence of magnetization of 2D VS_2 ultrathin nanosheet at 300 K, where the PM signals have been deduced. Inset: enlarged central section of (b). c) Temperature-dependent resistivity of VS_2 nanosheets under various magnetic fields. d) Magnetic-field-dependent of the magnetoresistance for VS_2 nanosheets at 100 K (purple) and 300 K (blue), both showing negative magnetoresistance.

in Figure S7, Supporting Information), and the inverse susceptibility exhibited nonparamagnetic behavior even at room temperature (**Figure 3**a), indicating the arisen of magnetic ordering of 2D VS_2 after vdW interaction engineering. Further evidence for the room-temperature ferromagnetism was provided by the *M–H* curves of the 2D VS_2 at 300 K (Figure 3b). The S-shaped *M–H* curve with a typical hysteresis loop of 2D VS_2 at 300 K clearly reveals ferromagnetism. The appearance of magnetization here was mainly attributed to the quantum mechanical confinement in 2D VS_2. The decoupling of interlayer interaction via the weakening of vdW bonds leads to a decrease in the covalency of V-S bond, which is in favor of V^{4+} ionicity and electron localization. Benefited from the localized odd electron in 3d orbital of V^{4+} and the effective ferromagnetic coupling mechanism in VS_2 monolayer,[6] few-layered VS_2 hence exhibit an enhanced ferromagnetic character. The temperature-dependent resistivity curves under some selective magnetic fields as shown in Figure 3c display a negative temperature coefficient of resistivity, and manifest negative magnetoresistance (MR) (i.e., the resistivity is substantially suppressed under external magnetic field). Considering the positive temperature coefficient of resistivity in thicker VS_2 lamella that obtained by NH_3 assisted exfoliation[12a] as well as the metal behavior in bulk VS_2, the negative temperature coefficient of resistivity in 2D VS_2 sample further indicated the effective bandgap opening by vdW interaction engineering. Noting here that the abnormity in the vicinity of 250 K is charge-density-wave (CDW) ordering transition.[12b] As presented in Figure 3d, the value of MR in 2D VS_2 reached ≈13% at 100 K, 5 T. The MR effect further illustrates the existence of magnetism in 2D VS_2. It can be found that the field-dependent MR and magnetization curves similarly exhibit two distinct regions: a rapid increase with the magnetic field below 5000 Oe, and a much slower increase above 5000 Oe as shown in Figure S8 (Supporting Information). These results indicate that under either the low- or high-field, the MR and the magnetization behaviors are closely correlated. Above mentioned results clearly indicate that the elimination of interlayer coupling would lead to the opening of bandgap with the ferromagnetic ground state well kept, bringing a room-temperature intrinsic ferromagnetic semiconductor among pristine TMDCs.

The weakening of vdW interactions in layered VS_2 also presents alternative opportunity for precise manipulation of the electronic states, which can be realized through compression.[13] Following this line, we demonstrate round control of the electronic states by applying hydrostatic pressure in a diamond anvil cell (DAC) (**Figure 4**a). In situ XRD spectra (Figure S10 and S11, Supporting Information) have successfully monitored the change of lattice parameters with the increment in pressure (see Methods in the Supporting Information for details). For the experimental range, all existing peaks can be indexed to the same space group ($P3\overline{m}\ 1$). On the basis of hexagonal 1T VS_2 model, the lattice parameters for few-layered VS_2 were determined under different pressures, as presented in Figure S12 and Table S1 (Supporting Information). Both the in-plane and out-of-plane lattice constants were reduced

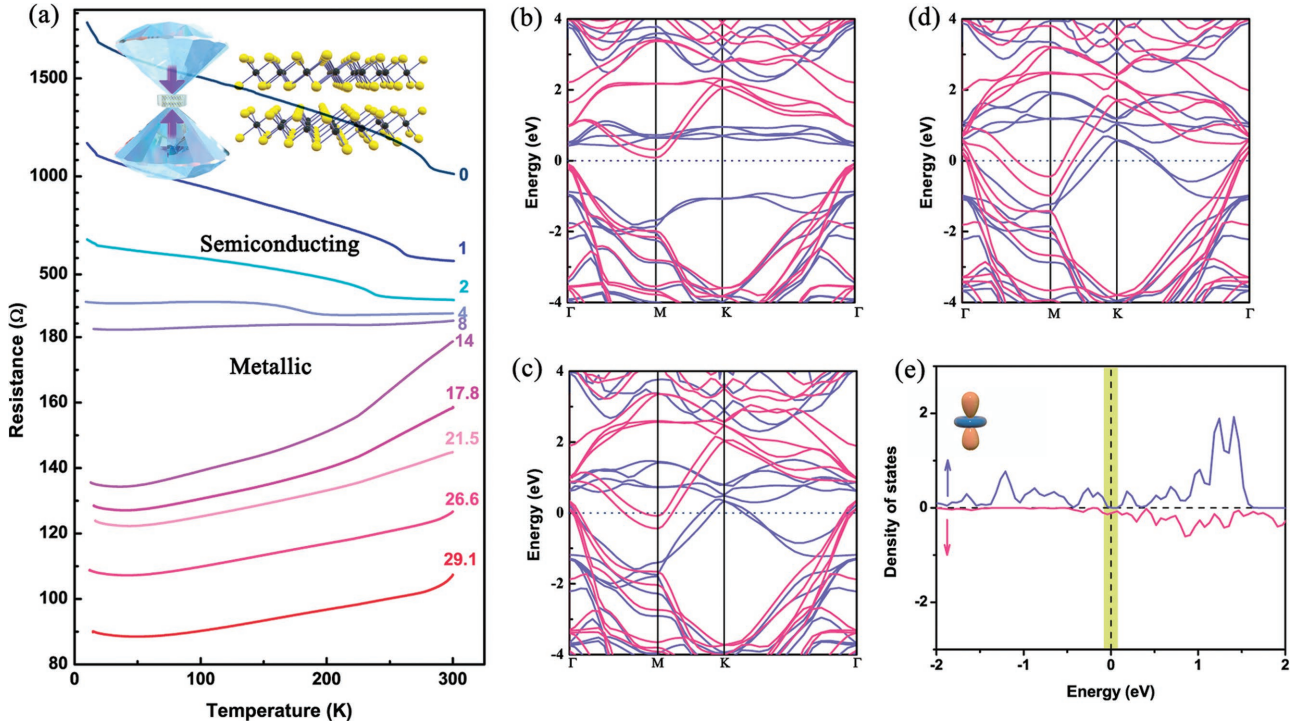

Figure 4. Pressure-induced metallization in 2D VS_2 and theoretical calculated electronic structure. a) Temperature-dependent resistivity curves at different pressures. Each colored line represents one resistivity curve with the number that represents the pressure in GPa: 2D VS_2 evolves from semiconductor to metal at a high pressure of ≈5 GPa. A schematic set up of the high-pressure diamond anvil cell (DAC) and a side view of 2D VS_2 at ambient pressure are also presented. (b)–(d) are calculated spin-resolved band structures of 2D VS_2 nanosheets: b) ambient pressure, c) 5.64 GPa, and d) 18.68 GPa. The spins are represented in different colors: blue represents the "↑" states while red represents the "↓" states. e) Projected density of states (PDOS) of d orbital at 5.64 GPa. All calculations were based on cell parameters obtained from high-pressure in situ XRD measurements.

under high hydrostatic pressure. In comparison, cell parameter c is more severely affected, with a reduction of up to ≈12% under 18.68 GPa, since the weak vdW bondings are more compressible. Selected area electron diffraction (see Figure S9, Supporting Information) patterns for 2D VS_2 nanosheets confirmed that the crystallinity and hexagonal symmetry were not significantly affected after compression, indicating that the structure could be basically recovered back after the high-pressure experiments. For exploring the effect of hydrostatic pressure on the electronic states of 2D VS_2, in situ temperature-dependent resistivity measurements were carried out at high pressures, which revealed a semiconductor-to-metal transition, as presented in Figure 4a. At lower pressures, 2D VS_2 nanosheets exhibited semiconducting behavior, in consistence with previous transport measurements. In this pressure region, we can obviously observer a CDW transition in the vicinity of 250 K from the R–T curve and the transition temperature drop as the pressure is increasing. The pressure caused the decrease of cell parameter which weakens CDW fluctuation.[16] At a pressure of ≈5 GPa, VS_2 nanosheets experienced an electronic state transition from semiconducting to metallic state, with the CDW transition being finally suppressed. Increasing pressure henceforth resulted in lower resistivity in 2D VS_2 nanosheets, of which the conductivity is over an order of magnitude higher than that at ambient conditions, supporting the metallic behavior. In a word, engineering of the vdW interactions has allowed round control of the electronic states in pristine VS_2, which paved the foundation for dual regulation of both spin properties and bandgap.

Density functional theory (DFT) calculations attribute the semiconductor-to-metallic state transition mostly to the d orbital states of vanadium. Based on the cell parameters obtained from the in situ XRD measurements, we performed ab initio calculations on the electronic structures of a bilayer VS_2 at three representative pressures as shown in Figure 4b–d; and Figure S13 (Supporting Information), which clearly demonstrates the evolution from semiconductor to metal. Seen from Figure 4b which is at ambient pressure, the valence band maximum lies ≈0.3 eV below E_F, in good agreement with the UPS measurement above, which lends support to the accuracy of our calculation model. V d orbitals mostly dominate the bottom of the conduction band, while the top of the valence band mostly originates from S p_x and p_y orbitals. As the pressure is increased to 5.64 GPa, the lattice structure of the VS_2 are adjusted to balance compression, resulting in V dz^2 contributing most to the density of states at E_F (Figure 4e, highlighted in green). The major reduction of cell parameter c allows dz^2 to gain more overlap with S p orbitals, which explains the wider dispersions that triggers metallization. Finally, when the pressure is increased to 18.68 GPa, the in-plane compression also partly contributes to the density of states at the Fermi level besides the axial compression that strengthens the overlapping of d orbitals, with the density of states from the S p orbital enhancement at E_F

(Figure S14, highlighted in green, Supporting Information). Based on the theoretical investigation, the transition metal, V, has played a dominant role for controlling the electronic state in VS_2, leading to a vdW interaction-dependent electronic band structure. Therefore, the pristine lattice of 2D VS_2 hence enabled modulation of the bandgap through vdW interaction engineering, making dual regulation of spin properties, and bandgap experimentally accessible.

In conclusion, we have experimentally realized intrinsic magnetic ordering in a pristine VS_2 lattice with a few-layered structure. Through vdW interactions engineering, few-layered VS_2 nanosheet was found to be a new class of ferromagnetic semiconductor, enabling dual regulation of spin properties and bandgap. Moreover, a decisive role of vdW interactions in determining the electronic states in 2D VS_2 was revealed, allowing round control of the electronic states of VS_2. In detail, enlarging of the vdW bonds would trigger a metal-to-semiconductor transition, while metallization would occur along with the compression of the vdW bonds. The pristine VS_2 lattice thus provides a new 2D platform for precise manipulation of both charge and spin degrees of freedom catering for spintronics based on TMDCs.

Supporting Information

Supporting Information is available from the Wiley Online Library or from the author.

Acknowledgements

Y.Q.G., H.T.D., and X.S. contributed equally to this work. This work was financially supported by the National Basic Research Program of China (No. 2015CB932302), the National Natural Science Foundation of China (Nos. 21501164, U1432133, U1632154, and J1030412), National Young Top-Notch Talent Support Program, the Anhui Provincial Natural Science Foundation (No. 1608085QA08), and the Fundamental Research Funds for the Central Universities (Nos. WK2060190027, WK2310000055, and WK2340000065).

Conflict of Interest

The authors declare no conflict of interest.

Keywords

2D materials, ferromagnetic TMDCs, hydrostatic pressure, metal-to-insulator transition, van der Waals interaction engineering

Received: February 5, 2017
Revised: April 21, 2017
Published online:

[1] a) Y. Zhang, Y.-W. Tan, H. L. Stormer, P. Kim, *Nature* **2005**, *438*, 201; b) A. K. Geim, I. V. Grigorieva, *Nature* **2013**, *499*, 419; c) M. Chhowalla, H. S. Shin, G. Eda, L.-J. Li, K. P. Loh, H. Zhang, *Nat. Chem.* **2013**, *5*, 263; d) Y. Jin, D. H. Keum, S.-J. An, J. Kim, H. S. Lee, Y. H. Lee, *Adv. Mater.* **2015**, *27*, 5534; e) X. Xu, W. Yao, D. Xiao, T. F. Heinz, *Nat. Phys.* **2014**, *10*, 343; f) J. N. Coleman, M. Lotya, A. O'Neill, S. D. Bergin, P. J. King, U. Khan, K. Young, A. Gaucher, S. De, R. J. Smith, I. V. Shvets, S. K. Arora, G. Stanton, H.-Y. Kim, K. Lee, G. T. Kim, G. S. Duesberg, T. Hallam, J. J. Boland, J. J. Wang, J. F. Donegan, J. C. Grunlan, G. Moriarty, A. Shmeliov, R. J. Nicholls, J. M. Perkins, E. M. Grieveson, K. Theuwissen, D. W. McComb, P. D. Nellist, V. Nicolosi, *Science* **2011**, *331*, 568.

[2] Y. Gong, J. Lin, X. Wang, G. Shi, S. Lei, Z. Lin, X. Zou, G. Ye, R. Vajtai, B. I. Yakobson, H. Terrones, M. Terrones, B. K. Tay, J. Lou, S. T. Pantelides, Z. Liu, W. Zhou, P. M. Ajayan, *Nat. Mater.* **2014**, *13*, 1135.

[3] a) Y. Wang, R. Fullon, M. Acerce, C. E. Petoukhoff, J. Yang, C. Chen, S. Du, S. K. Lai, S. P. Lau, D. Voiry, D. O'Carroll, G. Gupta, A. D. Mohite, S. Zhang, H. Zhou, M. Chhowalla, *Adv. Mater.* **2017**, *29*, 1603995; b) J. Wang, Q. Yao, C.-W. Huang, X. Zou, L. Liao, S. Chen, Z. Fan, K. Zhang, W. Wu, X. Xiao, C. Jiang, W.-W. Wu, *Adv. Mater.* **2016**, *28*, 8302; c) M. Acerce, D. Voiry, M. Chhowalla, *Nat. Nanotechnol.* **2015**, *10*, 313; d) D. H. Keum, S. Cho, J. H. Kim, D.-H. Choe, H.-J. Sung, M. Kan, H. Kang, J.-Y. Hwang, S. W. Kim, H. Yang, K. J. Chang, Y. H. Lee, *Nat. Phys.* **2015**, *11*, 482.

[4] F. Körmann, B. Grabowski, P. Söderlind, M. Palumbo, S. G. Fries, T. Hickel, J. Neugebauer, *J. Phys.: Condens. Matter* **2013**, *25*, 425401.

[5] M. Venkatesan, C. B. Fitzgerald, J. M. D. Coey, *Nature* **2004**, *430*, 630.

[6] Y. Ma, Y. Dai, M. Guo, C. Niu, Y. Zhu, B. Huang, *ACS Nano* **2012**, *6*, 1695.

[7] a) A. Ramasubramaniam, D. Naveh, *Phys. Rev. B* **2013**, *87*, 195201; b) B. Yang, H. Zheng, R. Han, X. Dua, Y. Yan, *RSC Adv.* **2014**, *4*, 54335; c) A. N. Andriotis, M. Menon, *Phys. Rev. B* **2014**, *90*, 125304; d) K. Dolui, A. Narayan, I. Rungger, S. Sanvito, *Phys. Rev. B* **2014**, *90*, 041401.

[8] a) S. W. Han, Y. H. Hwang, S.-H. Kim, W. S. Yun, J. D. Lee, M. G. Park, S. Ryu, J. S. Park, D.-H. Yoo, S.-P. Yoon, S. C. Hong, K. S. Kim, Y. S. Park, *Phys. Rev. Lett.* **2013**, *110*, 247201; b) Z. Zhang, X. Zou, V. H. Crespi, B. I. Yakobson, *ACS Nano* **2013**, *7*, 10475.

[9] a) L. Cai, J. He, Q. Liu, T. Yao, L. Chen, W. Yan, F. Hu, Y. Jiang, Y. Zhao, T. Hu, Z. Sun, S. Wei, *J. Am. Chem. Soc.* **2015**, *137*, 2622; b) Y. Cheng, Z. Guo, W. Mi, U. Schwingenschlögl, Z. Zhu, *Phys. Rev. B* **2013**, *87*, 100401.

[10] H. Zheng, B. Yang, D. Wang, R. Han, X. Du, Y. Yan, *Appl. Phys. Lett.* **2014**, *104*, 132403.

[11] a) D. D. Awschalom, M. E. Flatté, *Nat. Phys.* **2007**, *3*, 153; b) S. A. Wolf, D. D. Awschalom, R. A. Buhrman, J. M. Daughton, S. von Molnár, M. L. Roukes, A. Y. Chtchelkanova, D. M. Treger, *Science* **2001**, *294*, 1488.

[12] a) J. Feng, X. Sun, C. Wu, L. Peng, C. Lin, S. Hu, J. Yang, Y. Xie, *J. Am. Chem. Soc.* **2011**, *133*, 17832; b) M. Mulazzi, A. Chainani, N. Katayama, R. Eguchi, M. Matsunami, H. Ohashi, Y. Senba, M. Nohara, M. Uchida, H. Takagi, S. Shin, *Phys. Rev. B* **2010**, *82*, 075130; c) N. Katayama, M. Uchida, D. Hashizume, S. Niitaka, J. Matsuno, D. Matsumura, Y. Nishihata, J. Mizuki, N. Takeshita, A. Gauzzi, M. Nohara, H. Takagi, *Phys. Rev. Lett.* **2009**, *103*, 146405; d) L.-Y. Gan, Q. Zhang, Y. Cheng, U. Schwingenschlögl, *Phys. Rev. B* **2013**, *88*, 235310.

[13] a) A. P. Nayak, S. Bhattacharyya, J. Zhu, J. Liu, X. Wu, T. Pandey, C. Jin, A. K. Singh, D. Akinwande, J.-F. Lin, *Nat. Commun.* **2014**, *5*, 3731; b) Z. Zhao, H. Zhang, H. Yuan, S. Wang, Y. Lin, Q. Zeng, G. Xu, Z. Liu, G. K. Solanki, K. D. Patel, Y. Cui, H. Y. Hwang, W. L. Mao, *Nat. Commun.* **2015**, *6*, 7312; c) Z.-H. Chi, X.-M. Zhao,

H. Zhang, A. F. Goncharov, S. S. Lobanov, T. Kagayama, M. Sakata, X.-J. Chen, *Phys. Rev. Lett.* **2014**, *113*, 036802.

[14] D. LeBoeuf, N. Doiron-Leyraud, J. Levallois, R. Daou, J.-B. Bonnemaison, N. E. Hussey, L. Balicas, B. J. Ramshaw, R. Liang, D. A. Bonn, W. N. Hardy, S. Adachi, C. Proust, L. Taillefer, *Nature* **2007**, *450*, 533.

[15] a) C. Lin, X. Zhu, J. Feng, C. Wu, S. Hu, J. Peng, Y. Guo, L. Peng, J. Zhao, J. Huang, J. Yang, Y. Xie, *J. Am. Chem. Soc.* **2013**, *135*, 5144; b) C. Kittel, *Introduction to Solid State Physics*, 8th ed., Wiley, New York **2005**.

[16] B. Sipos, A. F. Kusmartseva, A. Akrap, H. Berger, L. Forró, E. Tutis, *Nat. Mater.* **2008**, *7*, 960.